Acta Cryst. (1996). B52, 440–449

Structural Chemistry of $NaCoPO_4$

ROBERT HAMMOND* AND JACQUES BARBIER

Department of Chemistry, McMaster University, 1280 Main Street West, Hamilton, Ontario, Canada L8S 4M1. E-mail: rhammond@miranda.chemistry.mcmaster.ca

(Received 8 August 1995; accepted 30 November 1995)

Abstract

Sodium cobalt phosphate, $NaCoPO_4$, occurs as two different polymorphs which transform reversibly at 998 K. The crystal structures of both polymorphs have been determined by single crystal X-ray diffraction. The low-temperature form α-$NaCoPO_4$ crystallizes in the space group *Pnma* with cell parameters: a = 8.871 (3), b = 6.780 (3), c = 5.023 (1) Å and $Z = 4$ [$wR(F^2) = 0.0653$ for all 945 independent reflections]. The α-phase contains octahedrally coordinated Co and Na atoms and tetrahedrally coordinated P atoms, and is isostructural with maracite, $NaMnPO_4$. The structure of high-temperature β-$NaCoPO_4$ is hexagonal with space group $P6_5$ and cell parameters: a = 10.166 (1), c = 23.881 (5) Å and $Z = 24$ [$wR(F^2) = 0.0867$ for 4343 unique reflections]. The β-phase belongs to the large family of stuffed tridymites, with the P and Co atoms occupying tetrahedral sites and the Na atoms located in the cavities of the tetrahedral framework. The long c axis corresponds to a $3\times$ superstructure of the basic tridymite framework ($c \simeq 8$ Å) and is caused by the displacement of the Na atoms, tetrahedral tilts and strong distortions of the CoO_4 tetrahedra. A bond-valence analysis of these phases reveals that the polymorphism in $NaCoPO_4$ is due in part to over-/underbonding of the Na atom in the low-/high-temperature structures, respectively.

1. Introduction

During his study of the crystal chemistry of some $M^{I}M^{II}PO_4$ phosphates, Engel (1976) divided the compounds he examined into two broad groups. The first group consisted of those phases with structures based on Na_2SO_4 and Ca_2SiO_4 (*e.g.* $NaCdPO_4$, $NaMnPO_4$, $NaFePO_4$, $NaCaPO_4$ and $NaHgPO_4$), while the second was made up of phases with stuffed-tridymite structures (*e.g.* $NaZnPO_4$, $KZnPO_4$, $AgZnPO_4$ and $KCoPO_4$). While many of the compounds studied were polymorphic, $NaCoPO_4$ was unique in that the low-temperature α-phase belonged to the first group and the high-temperature β-phase was a member of the second. Based on the results of powder X-ray diffraction and IR and Raman spectroscopies, Paques-Ledent (1972, 1973, 1974) had previously assigned a phenacite structure to β-$NaCoPO_4$. This assignment, however, was questionable as no unit-cell data were provided for the high-temperature phase and it required that the Na ions would occur in an unusual tetrahedral coordination. Both Paques-Ledent and Engel reported that α-$NaCoPO_4$ is isostructural with $NaMnPO_4$ (maracite) and $NaFePO_4$. Structure determinations of $NaMnPO_4$ (Moring & Kostiner, 1986), $NaFePO_4$ (LePage & Donnay, 1977) and $Na(Fe,Zn)PO_4$ (Kabalov, Simonov & Belov, 1974) have confirmed that these three compounds are isostructural.

The reversible phase transition in $NaCoPO_4$, occurring at 998 K, is well documented and has been reported several times in the literature (Paques-Ledent, 1972, 1973, 1974; Engel, 1976; Kolsi, 1978), but no similar phase transition has been reported for $NaMnPO_4$ or $NaFePO_4$. Although Engel did observe an irreversible phase transition between the olivine form of $NaMnPO_4$ (natrophilite) and the maracite form, this is a consequence of the unusual cation arrangement found in natrophilite (Moore, 1972) and is not related to the $\alpha\rightarrow\beta$ phase transition in $NaCoPO_4$. Since no previous details of the structure of either polymorph of $NaCoPO_4$ have been reported, a determination of both crystal structures was undertaken and the results are reported here along with an argument about the origin of the phase transition.

2. Experimental

Powder samples of both polymorphs of $NaCoPO_4$ were prepared from stoichiometric mixtures of Na_2CO_3, $CoCO_3$ and $NH_4H_2PO_4$.* The samples were first heated to 773 K and held there for 16 h to pre-react the compounds and remove all the volatiles. The pre-reacted samples were then heated to 873 or 1023 K for 2–5 days and quenched in air to prepare the α- or β-phase, respectively. Single phase samples of both polymorphs were prepared and were confirmed by powder X-ray diffraction. DTA experiments on the α-phase sample confirmed the presence of the phase transition, which was observed at 999 K. A Guinier–Lenné camera with Fe $K\alpha_1$ radiation was used to obtain films of the powder

* Lists of anisotropic displacement parameters and structure factors have been deposited with the IUCr (Reference: BR0046). Copies may be obtained through The Managing Editor, International Union of Crystallography, 5 Abbey Square, Chester CH1 2HU, England.

Table 1. *Experimental details*

	α-$NaCoPO_4$	β-$NaCoPO_4$
Crystal data		
Chemical formula	$NaCoPO_4$	$NaCoPO_4$
Chemical formula weight	176.89	176.89
Cell setting	Orthorhombic	Hexagonal
Space group	*Pnma*	$P6_5$
a (Å)	8.871 (3)	10.1660 (10)
b (Å)	6.780 (3)	10.1660 (10)
c (Å)	5.0230 (10)	23.881 (5)
V (Å^3)	302.1 (2)	2137.4 (5)
Z	4	24
D_x (Mg m^{-3})	3.889	3.298
Radiation type	Ag $K\alpha$	Ag $K\alpha$
Wavelength (Å)	0.56086	0.56086
No. of reflections for cell parameters	20	26
θ range (°)	1.5–10	4.95–7.97
μ (mm^{-1})	3.189	2.704
Temperature (K)	293 (2)	293 (2)
Crystal form	Square prism	(110) twinned, irregular prism
Crystal size (mm)	0.14 × 0.11 × 0.05	0.34 × 0.27 × 0.15
Crystal colour	Orange–pink	Dark blue
Data collection		
Diffractometer	Siemens *R3m/V* diffractometer	Siemens *R3m/V* diffractometer
Data collection method	θ–2θ scan	θ–2θ scan
Absorption correction	Empirical from ψ-scans	Empirical from ψ-scans
T_{min}	0.515	0.652
T_{max}	0.587	0.967
No. of measured reflections	1812	8766
No. of independent reflections	945	4343
No. of observed reflections	598	3117
Criterion for observed reflections	$I > 2\sigma(I)$	$I > 2\sigma(I)$
R_{int}	0.0370	0.0442
θ_{max} (°)	30.02	30.08
Range of h, k, l	$0 \rightarrow h \rightarrow 15$ $0 \rightarrow k \rightarrow 12$ $-8 \rightarrow l \rightarrow 8$	$-13 \rightarrow h \rightarrow 15$ $0 \rightarrow k \rightarrow 15$ $0 \rightarrow l \rightarrow 42$
No. of standard reflections	3	3
Frequency of standard reflections	Every 100 reflections	Every 100 reflections
Refinement		
Refinement on	F^2	F^2
$R[F^2 > 2\sigma(F^2)]$	0.0308	0.0456
$wR(F^2)$	0.0603	0.0794
S	0.936	1.024
No. of reflections used in refinement	945	4343
No. of parameters used	41	254
H-atom treatment	H-atom parameters not refined	H-atom parameters not refined
Weighting scheme	$w = 1/[\sigma^2(F_o^2) + (0.0269P)]$, where $P = (F_o^2 + 2F_c^2)/3$	$w = 1/[\sigma^2(F_o^2) + (0.0377P)]$, where $P = (F_o^2 + 2F_c^2)/3$
$(\Delta/\sigma)_{max}$	0.001	0.001
$\Delta\rho_{max}$ (e Å^{-3})	0.749	0.922
$\Delta\rho_{min}$ (e Å^{-3})	−0.637	−0.938
Extinction method	*SHELXL*93 (Sheldrick, 1993)	None
Extinction coefficient	0.0343 (29)	–
Source of atomic scattering factors	*International Tables for Crystallography* (1992, Vol. C, Tables 4.2.6.8 and 6.1.1.4)	*International Tables for Crystallography* (1992, Vol. C, Tables 4.2.6.8 and 6.1.1.4)

patterns, which were then scanned using a KEJ-LS20 digital scanner. This instrument was also used for *in situ* observation of the phase transition. The α-$NaCoPO_4$ powder is pink in colour, while the β-$NaCoPO_4$ powder is dark blue.

Single crystals of the α-phase were grown using a flux method from a mixture of 3.32 g of α-$NaCoPO_4$ and 18.05 g of $Na_2Mo_4O_{13}$. The sample was soaked for 1 h at 953 K and then cooled at a rate of 3 K h^{-1} to a final temperature of 703 K. The $Na_2Mo_4O_{13}$ flux partially reacted with the $NaCoPO_4$ compound resulting in a mixture of at least three phases, with the small orange–pink crystals of α-$NaCoPO_4$ representing one of the minor products. Using precession photographs a suitable single crystal was selected for further study on a diffractometer.

Single crystals of β-$NaCoPO_4$ were readily obtained from a melt of $NaCoPO_4$, which was cooled at 1 K h^{-1} from 1223 to 1173 K. Powder X-ray diffraction patterns confirmed that the dark blue crystals obtained from the recrystallized melt were the same phase as the original powder sample. The crystals were again screened using precession photographs until a suitable candidate was found for data collection.

3. Data collection and structure refinement

The data collection for both α-$NaCoPO_4$ and β-$NaCoPO_4$ was performed on a Siemens *R3m/V* diffractometer system (Siemens, 1989) using Ag $K\alpha$ radiation. The cell refinement and data reduction were performed with *SHELXTL-Plus* (Sheldrick, 1991). Structure solution and refinement were effected using *SHELXS*86 (Sheldrick, 1990) and *SHELXL*93 (Sheldrick, 1993), respectively. Molecular graphics were rendered using *SHELXTL-Plus*. The raw data were empirically corrected for absorption using the psi-scan method. The structure solution of α-$NaCoPO_4$ was obtained using direct methods and the model obtained refined smoothly against F^2, first using isotropic and finally anisotropic atomic displacement parameters, to a final $wR(F^2)$ = 0.065. Details of the crystal data, data collection and structure refinement for the α- and β-phases are all listed in Table 1.

The structure solution for β-$NaCoPO_4$ was also obtained using direct methods, which located most of the Co and P atoms. The remaining atoms were located using electron-density difference maps during the refinement process. After locating all the atoms during the initial stages of the refinement, the isotropic atomic displacement parameters and the R indices remained quite high [$wR(F^2) \simeq 0.20$], suggesting the presence of twinning within the crystal. Drawing on the study of twin boundaries in $KLiSO_4$ (Klapper, Hahn & Chung, 1987), a (110) mirror plane was selected as the twin law: this was successful in improving the atomic displacement parameters and reducing the $wR(F^2)$ value, and refinement of the twin parameter indicated that the crystal contained 32.6 (1) vol-% of the twinned component. The refinement was carried out in both enantiomorphic space groups $P6_1$ and $P6_5$ with final anisotropic $wR(F^2)$ indices of 0.099 and 0.087, respectively. It was concluded that $P6_5$ was the correct space group choice for this particular crystal.

4. Description of the α-$NaCoPO_4$ structure

α-$NaCoPO_4$ is isostructural with $NaMnPO_4$ (maracite; Moring & Kostiner, 1986) and $NaFePO_4$ (LePage & Donnay, 1977). The final atomic coordinates and isotropic displacement parameters are listed in Table 2, while bond distances, angles and valences are given in Table 3. Based on the description of the $NaFePO_4$ structure given by LePage & Donnay (1977), α-$NaCoPO_4$ consists of edge-sharing chains of CoO_6 octahedra running parallel to the b axis, which are cross-connected by the PO_4 tetrahedra, giving rise to large ten-coordinate cavities in which the Na ions are located (see Fig. 1). The octahedral coordination of the Co ion shows significant variation in bond lengths and angles, with two compressed and two stretched bonds [bond valences 0.46 and 0.17, respectively, determined using the software package *STRUMO* (Brown, 1989)] and distortions in the O—Co—O bond angles from 76.30 to 93.74°. In the previous descriptions of $NaMnPO_4$ and $Na(Fe,Zn)PO_4$, the authors ignored the four long Na—O bonds (see Table 3) and considered the alkali ion to be in an octahedral coordination. These NaO_6 octahedra are also highly distorted as two of the bonds are very short (bond valence 0.27), while two others are longer than expected (bond valence 0.12), and the O—Na—O angles vary over a wide range, from 62.26 to 109.49°. The bond-valence sums (Table 3) show that the bonding in the PO_4 tetrahedron is well behaved. However, the octahedral Co^{2+} cation is slightly underbonded, while there is severe overbonding in the NaO_{10} polyhedron. Even if only the NaO_6 octahedron is considered the bond-valence sum is still 1.20, indicating that there is a strong compression in some of the Na—O bonds.

A calculation of the expected bond valences, based on the bond topology of the α-$NaCoPO_4$ structure, was performed using the method described by O'Keeffe (1989) and the results are also presented in Table 3. Using an octahedral Na coordination, the O(1) and O(2) atoms are bonded to two Na, two Co and one P, while

Table 2. *Fractional atomic coordinates and equivalent isotropic displacement parameters ($Å^2$) for α-$NaCoPO_4$*

$U_{eq} = (1/3)\Sigma_i\Sigma_j U_{ij} a_i^* a_j^* \mathbf{a}_i.\mathbf{a}_j$.

	x	y	z	U_{eq}
Na1	0.85208 (15)	1/4	0.5315 (3)	0.0166 (3)
Co1	1/2	1/2	1/2	0.01514 (11)
P1	0.17765 (8)	1/4	0.4621 (2)	0.00853 (14)
O1	0.1180 (2)	1/4	0.7495 (4)	0.0116 (4)
O2	0.3530 (2)	1/4	0.4516 (4)	0.0100 (3)
O3	0.1231 (2)	0.0661 (2)	0.3165 (3)	0.0141 (3)

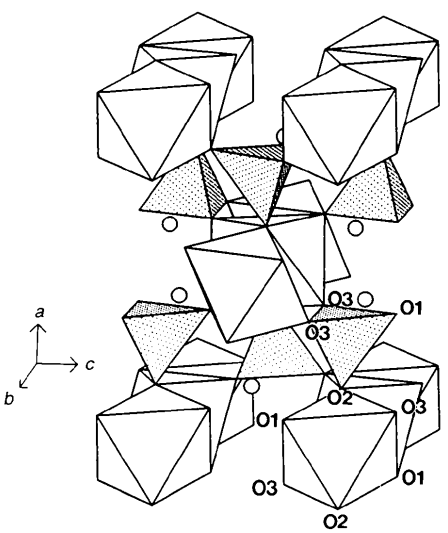

Fig. 1. The unit cell of α-$NaCoPO_4$ viewed along the [281] direction. The structure is made up of [010] rows of edge-sharing CoO_6 octahedra cross-linked by PO_4 tetrahedra with the Na ions, shown as open circles, fitting into cavities between these polyhedra.

Table 3. *Bond lengths (Å), angles (°) and valences for α-NaCoPO$_4$*

Observed bond valences were determined using the observed bond lengths and the software package *STRUMO* (Brown, 1989), while the calculated bond valences were obtained by the method described by O'Keeffe (1989).

CoO_6 octahedra

	Co	O3^{i}	O3^{ii}	O2	O2^{iii}	O1^{iv}	O1^{v}
O3^{i}	**1.980 (2)**						
O3^{ii}	180.00	**1.980 (2)**					
O2	86.26 (7)	93.74 (7)	**2.152 (2)**				
O2^{iii}	93.74 (7)	86.26 (7)	180.00	**2.152 (2)**			
O1^{iv}	88.80 (7)	91.20 (7)	76.30 (6)	103.70 (6)	**2.356 (2)**		
O1^{v}	91.20 (7)	88.80 (7)	103.70 (6)	76.30 (6)	180.00	**2.356 (2)**	

PO_4 tetrahedra

	P	O3	O3^{vi}	O1	O2
O3	**1.524 (2)**				
O3^{vi}	109.79 (12)	**1.524 (2)**			
O1	109.94 (8)	109.94 (8)	**1.538 (2)**		
O2	107.53 (8)	107.53 (8)	112.06 (12)	**1.556 (2)**	

NaO_{10} polyhedra

Na—O3^{vii}	2.285 (2)	Na—O3^{x}	2.285 (2)	Na—O1^{iv}	2.350 (3)
Na—O2^{viii}	2.426 (2)	Na—O2^{iv}	2.597 (2)	Na—O1^{xi}	2.601 (3)
Na—O3^{ix}	2.915 (2)	Na—O3^{xi}	2.915 (2)	Na—O3^{viii}	2.956 (2)
Na—O3^{ii}	2.956 (2)				

Observed bond valences

	Na	Co	P	Σ_{anion}
O1	0.23 + 0.12	0.17 (×2)	1.24	1.93
O2	0.19 + 0.12	0.29 (×2)	1.18	2.07
O3 (×2)	{0.27 (×2), 0.05 (×2), 0.04 (×2)}	0.46 (×2)	1.29 (×2)	2.07 (×2)
Σ_{cation}	1.38	1.84	5.00	

Calculated bond valences

O1	0.12 (×2)	0.29 (×2)	1.18	2.00
O2	0.12 (×2)	0.29 (×2)	1.18	2.00
O3 (×2)	0.26 (×2)	0.42 (×2)	1.32 (×2)	2.00 (×2)
Σ_{cation}	1.00	2.00	5.00	

Symmetry codes: (i) $\frac{1}{2}-x, y+\frac{1}{2}, z+\frac{1}{2}$; (ii) $x+\frac{1}{2}, \frac{1}{2}-y, \frac{1}{2}-z$; (iii) $1-x, 1-y, 1-z$; (iv) $x+\frac{1}{2}, y, \frac{3}{2}-z$; (v) $\frac{1}{2}-x, 1-y, z-\frac{1}{2}$; (vi) $x, \frac{1}{2}-y, z$; (vii) $1-x, -y, 1-z$; (viii) $x+\frac{1}{2}, y, \frac{1}{2}-z$; (ix) $x+1, \frac{1}{2}-y, z$; (x) $1-x, y+\frac{1}{2}, 1-z$; (xi) $x+1, y, z$.

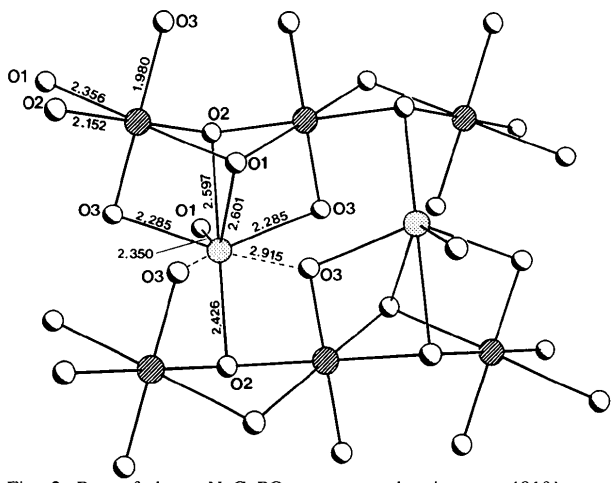

Fig. 2. Part of the α-NaCoPO$_4$ structure showing two [010] rows of CoO_6 octahedra joined *via* Na atoms. The PO_4 tetrahedra have been omitted for clarity. Note the irregular (6 + 4) Na coordination resulting from the shift of the Na atoms away from the shared faces of the CoO_6 and NaO_6 octahedra. The dashed lines represent two of the four long Na—O contacts. Also note the (010) mirror planes containing the Na, O(1) and O(2) atoms.

O(3) is bonded to only one Na, one Co and one P. Since the O(3) atom has fewer bonds, it is expected that each will be stronger, hence shorter, than those formed by O(1) and O(2) and this has a significant impact on the nature of the distortions in the coordination polyhedra in α-NaCoPO$_4$. A comparison of the observed and calculated bond valences shows several interesting results. First, all the *M*—O(3) bonds (*M* = Na, Co, P) show very good agreement between their observed and predicted values and all are clearly stronger than the *M*—O(1) and *M*—O(2) bonds, as predicted above. Second, the calculation fails to distinguish between O(1) and O(2), assigning identical bond valences for both oxygens. This shortcoming of the method was acknowledged by O'Keeffe in his original work and is a consequence of the identical bond topologies around the O(1) and O(2) positions in the structure. Third, it appears that the overbonding of the Na atoms is due to shorter than predicted Na—O(1) and Na—O(2) bonds (bond-valence values of 0.23 and 0.19, respectively, *versus* a predicted value of 0.12), while the slight underbonding of the Co atom is due to longer than

predicted Co—O(1) bonds (with a bond valence of 0.17 *versus* a predicted 0.29). These differences correspond to the accommodation of Na^+–Co^{2+} repulsions in the α-$NaCoPO_4$ structure. As shown in Fig. 2, each NaO_6 octahedron shares one face with each of a pair of adjacent CoO_6 octahedra, which moves the Na atom below the centre plane of the octahedron and away from the shared faces and the shared O(1)—O(2) edge, resulting in the shortening of one Na—O(1) bond (at 2.350 Å) and an Na—O(2) bond (at 2.426 Å). The large increase in the Na—O(1) bond strength is compensated by a comparable decrease in the Co—O(1) bond strength (see Table 3). These distortions do not alter the bond topology of the structure and so the calculation treats each type of *M*—O(1) and *M*—O(2) bond as equivalent. Finally, the shift of the Na atom brings it closer to the O(3) atoms of adjacent octahedral chains (see Fig. 2), resulting in the formation of four weak Na—O(3) bonds (bond valence = 0.05) which further increase the Na overbonding.

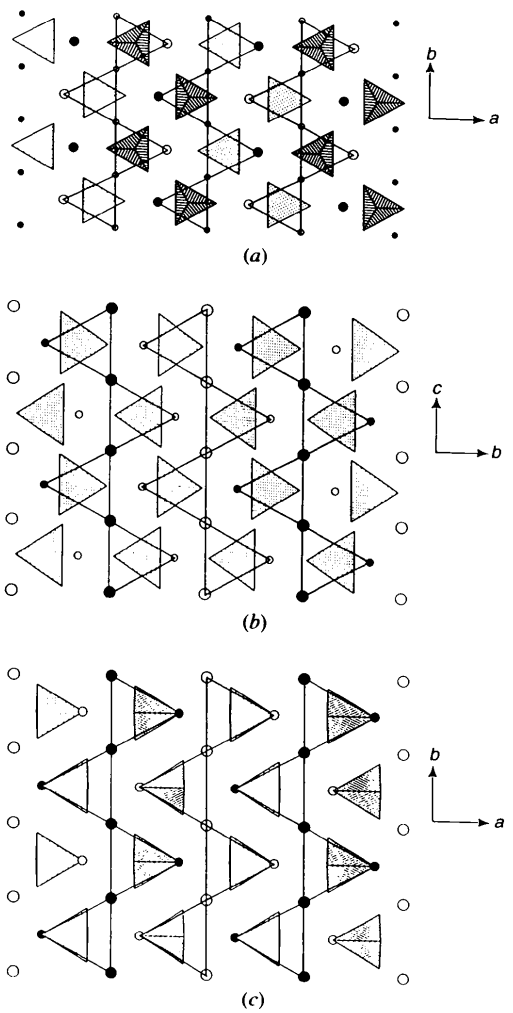

Fig. 3. Cation arrays for (*a*) $LiMgAsO_4$, (*b*) $LiMgVO_4$ and (*c*) α-$NaCoPO_4$. The small and large circles represent the alkali and M^{II} atoms, respectively, with filled and open circles at heights 0 and 50, respectively. The drawing emphasizes that all three structures are built up of serrated sheets of trigonal prisms of M^{I} and M^{II} cations and tetrahedral units.

Table 4. *Fractional atomic coordinates and equivalent isotropic displacement parameters (Å^2) for β-$NaCoPO_4$*

$U_{eq} = (1/3)\Sigma_i\Sigma_j U_{ij} a_i^* a_j^* \mathbf{a}_i.\mathbf{a}_j.$

	x	*y*	*z*	U_{eq}
Na1	0.0318 (4)	0.0379 (4)	0.0887 (2)	0.0392 (8)
Na2	0.9633 (4)	0.5110 (3)	0.08741 (14)	0.0291 (7)
Na3	0.5329 (3)	0.0475 (3)	0.08716 (11)	0.0181 (5)
Na4	0.5596 (3)	0.4949 (3)	0.08139 (13)	0.0248 (6)
Co1	0.34251 (9)	0.67147 (10)	0.14977 (4)	0.01395 (13)
Co2	0.68563 (10)	0.85143 (10)	0.01533 (3)	0.0163 (2)
Co3	0.20792 (9)	0.38073 (10)	0.04185 (3)	0.0133 (2)
Co4	0.18404 (9)	0.88352 (9)	0.01197 (3)	0.01396 (15)
P1	0.3279 (2)	0.6876 (2)	0.01435 (6)	0.0115 (3)
P2	0.6895 (2)	0.8364 (2)	0.14593 (6)	0.0122 (3)
P3	0.2161 (2)	0.3484 (2)	0.17330 (6)	0.0112 (3)
P4	0.2118 (2)	0.8820 (2)	0.14400 (6)	0.0113 (3)
O1	0.7163 (5)	0.2037 (6)	0.0254 (2)	0.0176 (9)
O2	0.6298 (6)	0.2652 (6)	0.9074 (2)	0.0221 (9)
O3	0.2672 (5)	0.8137 (5)	0.8471 (2)	0.0202 (9)
O4	0.6681 (5)	0.1475 (5)	0.6716 (2)	0.0194 (9)
O5	0.7042 (5)	0.9936 (5)	0.1361 (2)	0.0181 (9)
O6	0.0576 (5)	0.2066 (5)	0.1685 (2)	0.0185 (9)
O7	0.2383 (6)	0.9174 (6)	0.7560 (2)	0.0269 (11)
O8	0.4826 (5)	0.8323 (5)	0.0134 (2)	0.0233 (10)
O9	0.6785 (5)	0.9912 (5)	0.8839 (2)	0.0167 (8)
O10	0.5507 (5)	0.2199 (5)	0.1554 (2)	0.0191 (9)
O11	0.1957 (5)	0.1885 (5)	0.0130 (2)	0.0172 (9)
O12	0.6159 (6)	0.9152 (6)	0.7827 (2)	0.0217 (10)
O13	0.2698 (5)	0.9536 (5)	0.0868 (2)	0.0208 (9)
O14	0.9719 (5)	0.8331 (5)	0.0107 (2)	0.0224 (10)
O15	0.3265 (5)	0.0595 (5)	0.9696 (2)	0.0178 (9)
O16	0.2164 (5)	0.7205 (5)	0.9821 (2)	0.0201 (9)

It has previously been observed that the olivine-type $LiMgAsO_4$ and Na_2CrO_4-type $LiMgVO_4$ compounds have similar cation arrays, which can be described as serrated sheets of AsO_4-centred Li_4Mg_2 trigonal prisms and VO_4 centred Li_2Mg_4 trigonal prisms, respectively (Figs. 3*a* and *b*; Barbier, 1992). The different orientations of the TO_4 tetrahedra are a result of the variation in the two anion arrays of these compounds. The maracite-type structure of α-$NaCoPO_4$ can be described in a similar fashion, as shown in Fig. 3(*c*). It is built up from PO_4-centred Na_2Co_4 trigonal prisms which are sharing faces and edges along the [001] and [010] direction, respectively, thus forming similar serrated sheets parallel to the (100) plane. Accordingly, the structure of α-$NaCoPO_4$ is closely related to that of $LiMgVO_4$, both having similar cation arrays while differing in the arrangement of the anions as demonstrated by the different orientations of the TO_4 tetrahedra.

5. Description of the crystal structure of β-$NaCoPO_4$

The final atomic coordinates and equivalent isotropic displacement parameters for β-$NaCoPO_4$ are listed in Table 4, and bond distances, angles and valences are

listed in Table 5. The β-phase is a stuffed tridymite-type structure which is based on an ordered framework of corner-sharing CoO_4 and PO_4 tetrahedra, which form six-membered rings into which the Na atoms are 'stuffed'. These rings form channels parallel to the c axis by sharing the apical oxygens of the tetrahedra in adjacent rings, as shown in Figs. 4 and 5.

The bond lengths for the CoO_4 tetrahedra range from 1.932 to 2.016 Å, while those of the P—O bonds are more uniform (1.521–1.533 Å). Similarly, the O—Co—O bond angles show a wider range (97.0–131.9°) than the O—P—O angles (104.4–113.6°). These results indicate that the CoO_4 tetrahedra are very distorted in the β-phase, while the more strongly bonded PO_4 tetrahedra are almost regular. This distortion is greatest for $Co(3)O_4$: the four tetrahedral bonds are longer on average than in the other three CoO_4 tetrahedra (see Table 5) and there is in fact a longer fifth contact, Co(3)—O(2) at 2.475 Å, which contributes significantly to the bond-valence sum and could therefore be considered as a valid bond. This alternative description results in a distorted trigonal bipyramid $Co(3)O_5$, which shares an edge with the $P(1)O_4$ tetrahedron (see Fig. 5). In the stuffed tridymite structure of α-$KMgPO_4$, Quarton (1995) has observed a similar situation in which one of the nominally tetrahedral Mg atoms has been

Table 5. *Bond lengths (Å), angles (°) and valences (calculated using the software package STRUMO; Brown, 1989) for β-$NaCoPO_4$*

CoO_4 tetrahedra					
Co1	O2^{i}	O4^{ii}	O1^{iii}	O3^{iv}	
O2^{i}	**1.932 (5)**				
O4^{ii}	102.6 (2)	**1.967 (5)**			
O1^{iii}	105.6 (2)	113.9 (2)	**1.967 (5)**		
O3^{iv}	131.85 (2)	98.4 92)	104.5 (2)	**1.982 (5)**	
Co2	O6^{v}	O5^{vi}	O8	O7^{iv}	
O6^{v}	**1.950 (5)**				
O5^{vi}	110.8 (2)	**1.971 (5)**			
O8	113.5 (2)	115.9 (2)	**1.975 (5)**		
O7^{iv}	117.2 (2)	97.7 (2)	100.6 (2)	**1.975 (5)**	
Co3	O9^{vii}	O12^{iv}	O10^{viii}	O11	O2^{i}
O9^{vii}	**1.963 (5)**				
O12^{iv}	110.1 (2)	**1.992 (5)**			
O10^{viii}	118.5 (2)	117.7 (2)	**1.999 (5)**		
O11	100.4 (2)	97.0 (2)	109.3 (2)	**1.999 (4)**	
O2^{i}	88.3 (2)	80.9 (2)	64.8 (2)	171.2 (2)	**2.475 (5)**
Co4	O15^{ix}	O13^{x}	O14	O16^{xi}	
O15^{ix}	**1.932 (5)**				
O13^{x}	116.5 (2)	**1.952 (5)**			
O14	98.6 (2)	100.0 (2)	**1.959 (5)**		
O16^{xi}	103.0 (2)	113.6 (2)	113.8 (2)	**1.977 (5)**	
PO_4 tetrahedra					
P1	O8	O10^{viii}	O16^{xi}	O2^{i}	
O8	**1.524 (5)**				
O10^{viii}	113.0 (3)	**1.534 (4)**			
O16^{xi}	107.4 (3)	110.3 (3)	**1.539 (5)**		
O2^{i}	113.3 (3)	104.4 (3)	108.3 (3)	**1.544 (5)**	
P2	O7^{iv}	O3^{iv}	O13^{iii}	O5	
O7^{iv}	**1.528 (5)**				
O3^{iv}	109.0 (3)	**1.539 (5)**			
O13^{iii}	109.6 (3)	110.1 (3)	**1.546 (5)**		
O5	109.1 (3)	111.0 (3)	108.0 (3)	**1.547 (4)**	
P3	O6	O1^{iii}	O9^{iv}	O12^{iv}	
O6	**1.538 (4)**				
O1^{iii}	110.6 (3)	**1.547 (4)**			
O9^{iv}	110.1 (3)	108.3 (3)	**1.552 (4)**		
O12^{iv}	110.2 (3)	109.0 (3)	108.5 (3)	**1.553 (5)**	
P4	O14	O11^{iii}	O15^{i}	O4^{ii}	
O14	**1.521 (5)**				
O11^{iii}	108.4 (3)	**1.522 (4)**			
O15^{i}	108.7 (3)	110.0 (3)	**1.542 (4)**		
O4^{ii}	108.7 (3)	109.6 (3)	111.3 (3)	**1.543 (5)**	

Table 5 (*cont.*)

NaO_x polyhedra			
Na1—O11	2.415 (6)	Na1—O6	2.488 (6)
Na1—O13^{xii}	2.628 (6)	Na1—O6^{viii}	2.844 (6)
Na1—O13^{xiii}	2.857 (6)	Na1—O11^{xv}	2.864 (6)
Na1—O14^{xiv}	2.943 (6)		
Na2—O15^{xvi}	2.281 (5)	Na2—O9^{xvii}	2.343 (5)
Na2—O3^{xvii}	2.467 (6)	Na2—O8^{xv}	2.678 (7)
Na2—O2^{xvi}	2.691 (6)	Na2—O16^{xvii}	2.841 (6)
Na3—O1	2.283 (5)	Na3—O10	2.333 (5)
Na3—O14^{xiv}	2.348 (5)	Na3—O5^{xiv}	2.378 (5)
Na3—O8^{xiv}	2.652 (5)	Na3—O4^{xviii}	2.849 (6)
Na4—O16^{xvii}	2.263 (5)	Na4—O4^{xix}	2.323 (5)
Na4—O7^{iv}	2.360 (6)	Na4—O12^{iv}	2.444 (6)
Na4—O3^{xvii}	2.864 (6)		

	Na1	Na2	Na3	Na4	Co1	Co2	Co3	Co4	P1	P2	P3	P4	Σ_{anion}
O1			0.27		0.48						1.21		1.96
O2		0.09			0.52		0.12		1.22				1.95
O3		0.17			0.46					1.23			1.86
O4			0.06	0.27	0.48							1.22	2.03
O5			0.21			0.47				1.21			1.89
O6	0.16			0.06		0.50					1.24		2.02
	0.06												
O7				0.22		0.47				1.27			1.96
O8		0.09	0.10			0.47			1.28				1.94
O9		0.23					0.48				1.19		1.90
O10			0.24				0.44		1.25				1.93
O11	0.19						0.42					1.29	1.96
	0.06												
O12				0.18			0.44				1.19		1.81
O13	0.11							0.50		1.21			1.87
	0.06												
O14	0.05		0.23					0.49				1.30	2.07
O15		0.28						0.52				1.29	2.09
O16		0.06		0.29				0.46	1.23				2.04
Σ_{cation}	0.69	0.92	1.11	1.02	1.94	1.91	1.90	1.97	4.98	4.92	4.83	5.03	

Symmetry codes: (i) $y, y-x+1, z-\frac{5}{6}$; (ii) $1-x, 1-y, z-\frac{1}{2}$; (iii) $y, y-x+1, z+\frac{1}{6}$; (iv) $y-x, 1-x, z-\frac{2}{3}$; (v) $x-y+1, x+1, z-\frac{1}{6}$; (vi) $x-y+1, x, z-\frac{1}{6}$; (vii) $y-1, y-x, z-\frac{5}{6}$; (viii) $x-y, x, z-\frac{1}{6}$; (ix) $x, y+1, z-1$; (x) $x-1, y, z$; (xi) $x, y, z-1$; (xii) $x-1, y-1, z$; (xiii) $y-1, y-x, z+\frac{1}{6}$; (xiv) $x, y-1, z$; (xv) $y, y-x, z+\frac{1}{6}$; (xvi) $y+1, y-x+1, z-\frac{5}{6}$; (xvii) $y, y-x, z-\frac{5}{6}$; (xviii) $1-x, -y, z-\frac{1}{2}$; (xix) $y-x+1, 1-x, z-\frac{2}{3}$.

described as penta-coordinate. However, to simplify the description of the structure, the Co(3) atom will still be considered to have a tetrahedral coordination.

An examination of the ring topology shows that there are two types of rings present in the β-$NaCoPO_4$ structure. Using the definition made by Liebau (1985), each of the six tetrahedra in the ring either point up (*U*) or down (*D*) when viewed down the *c* axis. One quarter of the rings are centred around the Na1 atoms and have a regular *UDUDUD* arrangement, while the remaining rings around the Na2, Na3 and Na4 atoms have an *UUUDDD* topology. Both types of rings show a ditrigonal distortion (see Fig. 4) and furthermore the Na2, Na3 and Na4 atoms in the *UUUDDD* rings are clearly shifted away from the centre (by 0.45–0.65 Å), indicating that the channels are still too large for a symmetrical coordination. An examination of the bond-valence sums (Table 5) shows that the irregular coordination of these sites is satisfactory. The Na1 atoms in the *UDUDUD* rings do not have such an extreme displacement ($\sim$ 0.30 Å) and lie nearer to the centre of the ring. As a result of the longer Na(1)—O bonds (2.720 Å on average), this site is underbonded at room temperature, with a bond-valence sum of 0.69. The higher U_{eq} observed for this site (see Table 4) also indicates that the Na(1) atom is not strongly bound. It is likely that at temperatures above 998 K, *i.e.* in the stability field of the β-$NaCoPO_4$ structure, the thermal motion of the Na(1) atom within the ring provides a more satisfactory bonding.

One of the consequences of the Na atom's small size relative to the ring size is the formation of a pronounced $3\times$ superstructure along the *c* axis of the β-$NaCoPO_4$ structure. The layers of CoO_4 and PO_4 tetrahedra are not flat when viewed along the [110] direction (see Fig. 5), a result of both the size difference between the CoO_4 and PO_4 polyhedra and the severe tilting of the tetrahedra within each layer. It is also worth noting that each CoO_4 tetrahedron contains one short edge, indicated by the small (<100°) O—Co—O bond angles. In the coordination tetrahedra of Co(2), Co(3) and Co(4) these short edges are roughly aligned along the *c* axis, resulting in a compression of the structure along that direction, while in the Co(1) tetrahedron the short edge lies near the *ab* plane. Interestingly, although powder samples of β-$NaCoPO_4$ have been studied by several authors (Paques-

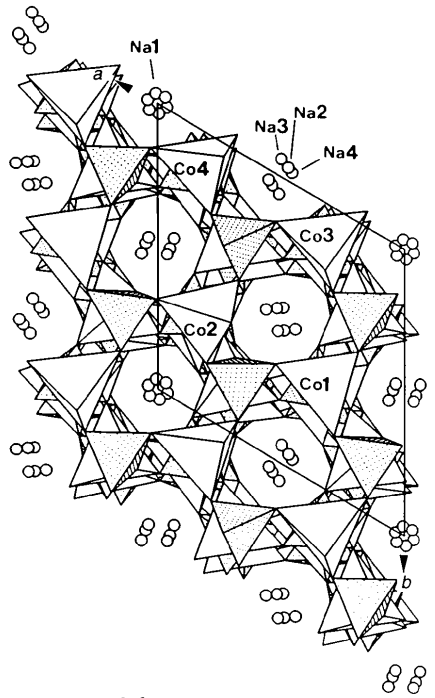

Fig. 4. The structure of β-$NaCoPO_4$ viewed down the [001] direction. The shaded and unshaded tetrahedra represent the PO_4 and CoO_4 units, respectively, and the Na atoms are shown as open circles. Notice the two types of six-membered rings (UDUDUD and UUUDDD) and the off-centre displacement of the Na atoms. The six-layer repeat along the c axis is generated by the 6_5 screw axis passing through the origin of the unit cell.

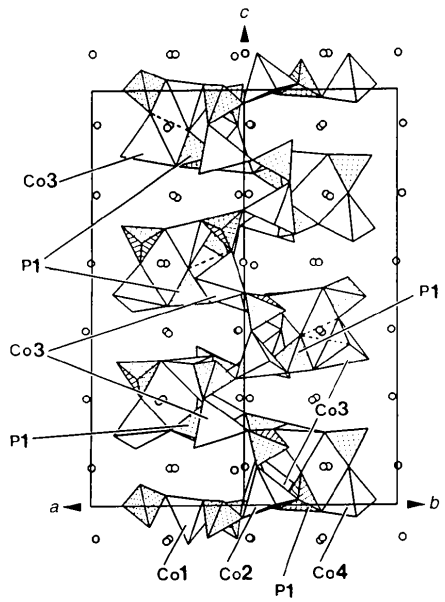

Fig. 5. The structure of β-$NaCoPO_4$ viewed down the [110] direction. The shaded and unshaded tetrahedra represent the PO_4 and CoO_4 units, respectively. The Na atoms are shown as open circles. The dashed lines show the extra edges of some of the $Co(3)O_5$ trigonal bipyramids (see text). Note the six layer repeat along the 23.68 Å c axis caused by tetrahedral tilting, layer buckling and shifts of the Na atoms.

Table 6. *The X-ray powder diffraction pattern for β-$NaCoPO_4$*

The calculated pattern was obtained using the program *XPOW* (Downs, Bartelmehs, Gibbs & Boison, 1993) using the atomic positions determined by the single crystal refinement. Unobserved lines for which $I_{calc} < 5.0$ are omitted for clarity.

h	k	l	d_{obs} (Å)	d_{calc} (Å)	I_{obs}	I_{calc}
1	0	3	5.9046	5.9052	14.8	36.2
2	0	0	4.4036	4.4042	46.9	66.5
1	1	3	4.2806	4.2853	3.0	0.4
2	0	2	4.1308	4.1320	2.7	7.4
0	0	6	3.9789	3.9793	45.0	56.3
2	0	3	3.8545	3.8535	16.7	26.8
1	2	1	3.2970	3.2974	10.7	8.6
2	1	1				2.4
2	0	5	3.2381	3.2974	6.5	9.1
1	0	7	3.1806	3.1808	8.5	13.9
1	1	6	3.1342	3.1339	4.3	5.3
1	2	3	3.0694	3.0713	40.5	24.4
2	1	3				12.7
2	0	6	2.9519	2.9526	100.0	100.0
3	0	1		2.9142		7.3
1	0	8	2.8262	2.8266	2.6	4.4
1	1	8		2.5740		7.8
2	2	0	2.5423	2.5428	77.9	68.3
1	0	9		2.5401		10.6
2	2	1	2.5284	2.5285	13.4	18.1
2	2	3	2.4224	2.4221	15.4	17.8
1	2	7	2.3829	2.3824	5.4	3.9
2	1	7				5.8
3	0	6	2.3628	2.3626	4.3	8.4
3	1	3		2.3354		6.5
2	0	9		2.2724		6.1
2	2	6	2.1426	2.1427	4.5	8.4
4	0	3	2.1225	2.1223	6.4	12.3
1	2	9	2.0748	2.0747	4.7	5.5
2	1	9				2.8
3	2	2	1.9928	1.9924	2.6	1.3
0	0	12		1.9896		5.8
4	0	6	1.9270	1.9267	5.2	10.8
1	2	11	1.8182	1.8182	4.3	1.1
2	1	11				0.1

Ledent, 1972, 1973, 1974; Engel, 1976; Kolsi, 1978), this 3× superstructure had not been reported previously. This is possibly because these powder X-ray diffraction studies have used copper radiation and consequently the weak superstructure reflections were masked by the strong fluorescence of the Co atoms. Table 6 reports the powder pattern observed using Fe $K\alpha_1$ radiation in addition to a pattern calculated using the atomic positions obtained from the single crystal X-ray refinement (software package *XPOW*; Downs, Bartelmehs, Gibbs & Boison Jr, 1993). The results show a reasonably good agreement between the observed and calculated patterns, with a large number of clearly observed superstructure reflections of the type (hkl, $l \neq 3n$).

6. The $\alpha \rightarrow \beta$ phase transition

The prominent feature of the crystal chemistry of $NaCoPO_4$ is the $\alpha \rightarrow \beta$ phase transition which occurs at 998 K and is accompanied by a significant decrease in the density [$D_x(\alpha) = 3.889\ g\ cm^{-3}$ *versus* $D_x(\beta) = 3.298\ g\ cm^{-3}$ at room temperature]. This is consistent

Table 7. *Bond valence sums, unit-cell volumes and global instability indices† (GII; Salinas-Sanchez, Garcia-Muñoz, Rodríguez-Carvajal, Saez-Puche & Martínez 1992) for maracite-type $NaM^{II}PO_4$ structures [M^{II} = Mn (Moring & Kostiner, 1986), Fe (LePage & Donnay, 1977), Co (this work)]*

Full coordination (CN = 10) was used for the Na atom in all three cases. The ionic radius of each cation (Shannon, 1976) is indicated in parentheses.

	Mn (0.96 Å)	Fe (0.92 Å)	Co (0.90 Å)
Na	1.14	1.26	1.38
M^{II}	1.94	1.92	1.84
P	4.92	4.94	5.00
O1	−1.89	−1.88	−1.91
O2	−2.06	−2.04	−2.06
O3	−2.03	−2.10	−2.11
V (Å^3)	320.84	311.1	302.11
GII†	0.09	0.13	0.18

† The global instability index is defined as the r.m.s. of the bond-valence sum deviations over all the atoms present in the asymmetric unit.

$$\mathrm{GII} = \left[\sum_{i=1}^{N}\left(\sum_{j} s_{ij} - V_j\right)^2 \Big/ N\right]^{1/2}$$

with the first-order character of the phase transition and its clearly reconstructive nature. It should be emphasized here that the large hexagonal unit cell determined for β-$NaCoPO_4$ has also been observed *in situ* at high temperatures by X-ray powder diffraction. The large $3xc$ hexagonal superstructure therefore corresponds to the true high-temperature phase and is not the result of a transformation occurring in the single crystals when they are quenched to room temperature.

Interestingly, similar phase transitions are not observed in the isostructural compounds $NaMnPO_4$ and $NaFePO_4$ (Engel, 1976). A bond-valence analysis across the series of structures $NaMnPO_4$, $NaFePO_4$ and α-$NaCoPO_4$, using the program *STRUMO* (Brown, 1989), provides an important clue to why this phase transition is only observed in $NaCoPO_4$. As the M^{II} cation decreases in size from Mn^{2+} to Fe^{2+} to Co^{2+}, it becomes increasingly underbonded, as shown in the bond-valence sums in Table 7, indicating that the cation is becoming too small for the octahedral site. At the same time a significant increase in the overbonding of the Na ion occurs. This overbonding corresponds to the compression of the Na—O bonds as a result of the decrease of the unit-cell volume caused by the decreasing M^{II} size across the series (*cf.* Table 7). The overall result is an increasing destabilization which can be evaluated by calculating the global instability index (GII; Salinas-Sanchez, Garcia-Muñoz, Rodríguez-Carvajal, Saez-Puche & Martínez, 1992) for each compound (see Table 7). As expected, there is a substantial increase in the GII from $NaMnPO_4$ to α-$NaCoPO_4$, confirming the destabilization of the maracite-type structure across the M^{II} = Mn, Fe, Co series. It has been proposed by Brown (1992) and Armbruster, Röthlisberger & Seifert (1990) that a GII greater than 0.2 would be sufficient to destabilize a structure at room temperature. The calculated value of the GII for α-$NaCoPO_4$, 0.18, is quite close to this threshold and may help explain why this compound undergoes a phase transition at elevated temperature.

The increasing destabilization of the maracite structure with decreasing M^{II} size reaches a critical level for M^{II} = Co. As the temperature is increased it is expected that the weaker Na—O bonds will tend to expand faster than the stronger Co—O and P—O bonds, thus further destabilizing the structure. Above 998 K, the thermal energy will be sufficient to induce a phase transition to the tridymite-type β-phase, which relieves the Na overbonding and removes the underbonding of Co (see Table 5). The results of the bond-valence calculations listed in Table 5 also show that, while the β-phase structure is generally well behaved, the Na(1) site is clearly underbonded (bond-valence sum = 0.69) and therefore the Na(1)—O bonds are stretched at room temperature. This underbonding is consistent with the stability of β-$NaCoPO_4$ at high temperature only. Coupled with the increase in density, this underbonding may also play a role in the reverse $\beta \rightarrow \alpha$ transition in which the structure transforms into the α-phase below 998 K.

The authors wish to acknowledge the assistance of the following: Dr J. Britten for X-ray data collection, F. Gibbs for the DTA experiments and the Natural Science and Engineering Research Council for financial support.

References

Armbruster, T., Röthlisberger, F. & Seifert, F. (1990). *Am. Miner.* **75**, 847–858.
Barbier, J. (1992). *Aust. J. Chem.* **45**, 1355–1362.
Brown, I. D. (1989). *J. Chem. Inf. Comput. Sci.* **29**, 266–271.
Brown, I. D. (1992). *Z. Krist.* **199**, 255–272.
Downs, R., Bartelmehs, K., Gibbs, G. & Boison Jr, M. (1993). *Am. Miner.* **78**, 1104–1107.
Engel, G. (1976). *Neues Jahrb. Mineral. Abh.* **127**, 197–211.
Kabalov, Y. K., Suminov, M. A. & Belov, N. (1974). *Dokl. Akad. Nauk. SSSR*, **216**, 1034–1036.
Klapper, H., Hahn, T. & Chung, S. J. (1987). *Acta Cryst.* **B43**, 147–159.
Kolsi, A.-W. (1978). *C. R. Acad. Sci. Paris Ser. C*, **286**, 249–251.
LePage, Y. & Donnay, G. (1977). *Can. Miner.* **15**, 518–521.
Liebau, F. (1985) *Structural Chemistry of Silicates*, pp. 260. New York: Springer-Verlag.
Moore, P. B. (1972). *Am. Miner.* **57**, 1333–1344.
Moring, J. & Kostiner, E. (1986). *J. Solid State Chem.* **61**, 379–383.
O'Keeffe (1989). *Struct. Bonding*, **71**, 161–190.
Paques-Ledent, M.-T. (1972). *C. R. Acad. Sci. Paris Ser. C*, **274**, 1998–2000.

Paques-Ledent, M.-T. (1973). *Rev. Chim. Miner.* **10**, 785–794.
Paques-Ledent, M.-T. (1974). *Ind. Chim. Belg.* **39**, 845–858.
Quarton, M. (1995). Private communication.
Salinas-Sanchez, A., Garcia-Muñoz, J. L., Rodríguez-Carvajal, J., Saez-Puche, R. & Martínez J. L. (1992). *J. Solid State Chem.* **100**, 201–211.
Shannon, R. D. (1976). *Acta Cryst.* A**32**, 751–767.
Sheldrick, G. M. (1990). *Acta Cryst.* A**46**, 467–473.
Sheldrick, G. M. (1991). *SHELXTL-Plus*. Release 4.1. Siemens Analytical X-ray Instruments Inc., Madison, Wisconsin, USA.
Sheldrick, G. M. (1993). *SHELXL*93. *Program for the Refinement of Crystal Structures*. University of Göttingen, Germany.
Siemens (1989). *R3m/V Crystallographic Research System*. Siemens Analytical X-ray Instruments Inc., Madison, Wisconsin, USA.